CHINESE OPTICS LETTERS

Vol. 21, No. 6 | June 2023

Optical scrambler using WGM micro-bottle cavity

Pengfa Chang (常朋发)[1], Chen Wang (王 晨)[1], Tao Jiang (蒋 涛)[1], Longsheng Wang (王龙生)[1], Tong Zhao (赵 彤)[1], Hua Gao (高 华)[1], Zhiwei Jia (贾志伟)[1], Yuanyuan Guo (郭园园)[1], Yuncai Wang (王云才)[2], and Anbang Wang (王安帮)[1,2*]

[1] Key Laboratory of Advanced Transducers & Intelligent Control Systems, Ministry of Education and Shanxi Province, College of Physics & Optoelectronic Engineering, Taiyuan University of Technology, Taiyuan 030024, China

[2] Guangdong Provincial Key Laboratory of Photonics Information Technology, School of Information Engineering, Guangdong University of Technology, Guangzhou 510006, China

*Corresponding author: wanganbang@tyut.edu.cn

Received January 28, 2023 | Accepted March 17, 2023 | Posted Online June 6, 2023

An optical scrambler using a whispering-gallery-mode (WGM) micro-bottle cavity to scramble a complex optical signal to generate an uncorrelated output is proposed. We experimentally demonstrated this micro-cavity scrambler by using chaotic laser light as the incident signal and studied the influence of the coupling state. Experiments achieved full scrambling with a low cross correlation of 0.028 between the output and the input. Results indicate that the scrambling effect originates from the interference among numerous WGMs in the bottle cavity. It is believed that the micro-bottle cavity with an efficient scrambling function can become a promising candidate for encryption.

Keywords: scrambler; encryption; whispering gallery mode; micro-bottle cavity; secure communication.
DOI: 10.3788/COL202321.060601

1. Introduction

Optical scramblers that scramble optical temporal waveform signals have significant applications in cryptography[1–4]. For example, applying a pair of optical scramblers on a public random signal can generate two identical private random signals for physical key distribution[5]. Furthermore, if the scrambling effect is irreversible, then optical scramblers can also be used for physical one-way functions[6]. Note that for above cryptography applications, dissimilarity between the input and the output of the optical scrambler is very important for security.

Scrambling can be realized by the nonlinear response in an optical or opto-electronic system, typically including semiconductor lasers[5,7–15] and optical dispersive devices[16–18]. For semiconductor lasers, the scrambling effect originates from the nonlinear laser dynamics induced by injecting input light and by delayed self-feedback[7]. Several types of semiconductor lasers, such as distributed feedback Bragg lasers[7–9], Fabry–Perot lasers[10,11], and vertical-cavity surface-emitting lasers[12,13], have been proved to have a scrambling effect. Unfortunately, for typical complex signals, such as chaotic light[8,12] and noise light[9,10], the input-output correlation values are still high and thus the scrambling effect needs to be improved. For example, amplitude-constant phase-random light[5,14] was proposed for reducing the input-output correlation of semiconductor lasers. Optical dispersive devices like chirped fiber Bragg gratings provide a scrambling scheme with low input-output correlation[18]. The main issue is that its simple hardware structure could be duplicated by an eavesdropper.

We notice that whispering-gallery-mode (WGM) microcavities have nonlinear feature responses due to nonuniform transmission spectra[19] and long photon lifetimes[20]. The nonuniform transmission causes the nonuniform filter effect, and the long lifetime of photons in the cavity makes more modes interfere. Thus, the scrambling effect of a WGM microcavity in a wide-spectrum input can be expected. Most recently, Jiang *et al.* used a WGM microsphere cavity and self-phase modulated feedback to generate broadband chaos[21]. Their work focused on chaos bandwidth and time-delay signature, but the input-output correlation was not studied, which is the basic feature for a scrambler.

In this Letter, we experimentally demonstrate an optical scrambler using a WGM micro-bottle cavity (MBC). Compared with the microsphere cavity, the MBC has a longer axis[22], which provides a more complex mode-field distribution and a broader coupling area. These features could generate high efficiency coupling and increase the number of modes, which are beneficial to the scrambling effect. To experimentally verify the scrambling effect of the MBC, a chaotic light is used as the input light. The scrambling effects, as well as the signal complexity at different coupling states, have been explored. Experimental results show that high-quality scrambling with a low input-output correlation near 0.03 can be achieved under the over-coupling state, accompanied by complexity enhancement.

2. Experimental Results and Discussion

The schematic diagram is shown in Fig. 1(a). An optical input signal is coupled into an MBC through a tapered fiber (TF) and then its temporal waveform is scrambled. The output signal thus has a waveform uncorrelated to the input. A verification experiment was carried out by using a chaotic light as the input signal. The experimental setup is shown in Fig. 1(b). The chaotic input light is generated by a distributed feedback Bragg (DFB) laser with optical feedback from an external mirror. In the feedback path, a polarization controller and an attenuator are used to adjust the polarization state and feedback strength, respectively. A proportion of the chaotic light, after being amplified by an erbium-doped fiber amplifier, is injected into the MBC through the TF. Note that the output waveform is sensitive to the polarization state of input light, and thus a polarization controller is inserted before the MBC. A 3 dB coupler taps into a portion of the input light, which, together with the output light, is detected using a real-time oscilloscope (Tektronix DPO73000, 30 GHz bandwidth) with photodetectors (Finisar XPDV2120RA, 40 GHz bandwidth).

The inset of Fig. 1(b) shows the photomicrograph of the MBC and the TF (the horizontal thin line). The MBC was made by pulling and discharging two sections of a single-mode fiber with a fiber fusion splicer. The maximum diameter and total length of the MBC are 120 μm and 700 μm, respectively. The intrinsic Q of the cavity is up to 10^7. The TF was made by pulling and heating a commercial single-mode fiber, and the thinnest diameter is about 1.6 μm. The bottle was set with an angle of about 34° to the TF. Both the TF and the MBC can be precisely positioned by 3-D positioning stages, and the coupling state can be adjusted.

The scrambling effect is characterized by the cross-correlation coefficient (CC) between the input and the output waveforms. The CC is defined as $\langle (I_x - \langle I_x \rangle)(I_y - \langle I_y \rangle) \rangle / \sigma_x \sigma_y$, where I_x and I_y are the time series of two signals, σ_x and σ_y are their standard deviations, and $\langle \cdot \rangle$ denotes the mean operator[23].

In our experiments, the DFB laser was biased at 80 mA (threshold current 23 mA), and its free-running wavelength was stabilized at 1548.822 nm using a temperature controller. The length of the feedback fiber path was about 16 m, and the corresponding feedback delay τ is about 80 ns. The optical feedback strength was adjusted to 0.2, calculated by the power ratio of the feedback light to the laser output. The chaotic light output from the DFB laser was used as the input signal, and its optical spectrum is shown in the gray line (red online) in Fig. 2(a). We further measured the MBC transmission spectrum as the wavelength-dependent transmissivity by scanning the wavelength of a tunable narrow-linewidth laser (Yenista-T100s, 400 kHz linewidth). The black line in Fig. 2(a) shows a transmission spectrum of the MBC, which was obtained with a coupling position close to the waist of the TF and an angle of about 34° between the MBC axis and the TF axis. There are many transmission lines with different heights, which are a kind of Fano-like line shape, that are introduced because of the large coupling loss[24,25]. Figure 2(b) plots the probability distribution of the transmission line heights. The transmittivity concentrates within the range from 0 to 0.2. The average transmission intensity (ATI) is calculated as 0.114, which is used to characterize the coupling strength between the TF and the MBC. As indicated in the transmission spectrum, each frequency component of the input light undergoes a different change. As a result, the scrambling effect will appear on the output signal.

Figure 3 shows the time-frequency characteristics of the input and output of the MBC under the coupling condition corresponding to Fig. 2. As shown in Fig. 3(a), the radio frequency (RF) spectrum of the input (blue online) is concentrated near the laser relaxation oscillation frequency. Clearly, the RF spectrum of the output light (red) becomes different. The low-frequency components are raised, and the peak at the relaxation frequency disappears. Moreover, the temporal waveforms of the input and the output are vastly different, as shown in Fig. 3(b). The CC between them is only calculated as 0.028, as shown in Fig. 3(c). The low correlation is also displayed in the scatter plot in the inset. The above results prove that the MBC scrambles the chaotic signal. There are no other peaks in the correlation except the time-delay signature of the feedback DFB laser, which indicates that in the output there is no intrinsic feature of the cavity.

Further, we calculate the permutation entropy (PE) to analyze whether there is complexity enhancement. The permutation

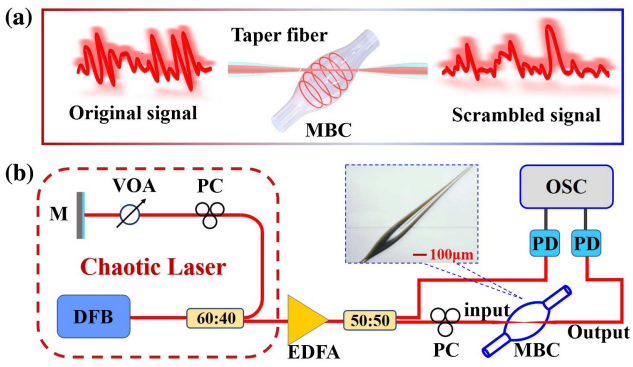

Fig. 1. (a) The schematic diagram of the scrambler using MBC and (b) the experimental setup. DFB, distributed-feedback laser; VOA, optical attenuator; PC, polarization controller; M, mirror; EDFA, erbium-doped fiber amplifier; MBC, micro-bottle cavity; PD, photodetector; OSC, oscilloscope. Inset: the coupling picture of the tapered fiber and the micro-bottle cavity.

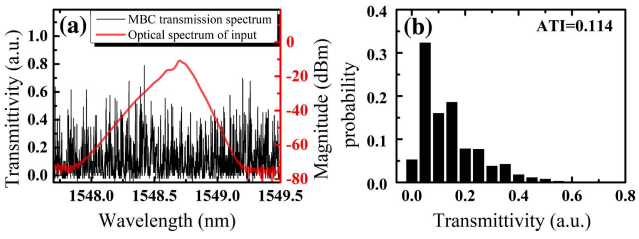

Fig. 2. (a) The transmission spectrum of the MBC (black) and the optical spectrum of the chaotic input (red line), (b) the probability distribution of the transmission intensity corresponding to (a). The ATI is calculated as the quotient of the summation of intensities on the spectrum divided by the number of data points.

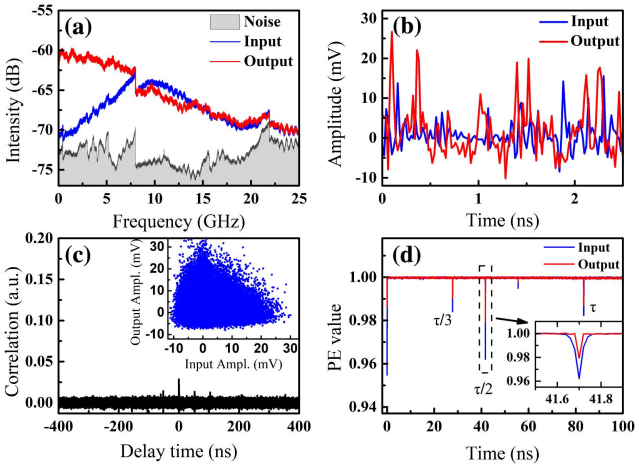

Fig. 3. (a) RF spectra, (b) time series, (c) cross correlation, and (d) permutation entropy curves of the input and output of the MBC. The light gray area in (a) represents the background noise. The inset in (c) shows the scatter plot between the input and output, and τ is the feedback delay of the chaotic laser.

entropy of the time series is calculated as $h_p = -(\Sigma(p(\pi_i) \times \ln p(\pi_i))/\ln(m!)$, where m is the embedding dimension, $p(\pi_i)$ is the ordinal pattern probability, and $i = 1, \ldots, m!$[26]. We chose $m = 4$ as Ref. [27] did. Note that the embedding delay t_e is required for phase-space reconstruction and will affect the PE because it changes elements of the reconstructed vectors. Figure 3(d) plots the PE as a function of the embedding delay of the input and output signals. Both curves have several minima locating at $\tau/3$, $\tau/2$, and τ, where τ is the feedback delay of the chaotic laser. The PE value is calculated by the average of all the minima. As a result, a small PE enhancement can be found from 0.9761 to 0.9855.

By fine adjusting the coupling point position along the axis of the TF, one can obtain different scrambling effects. Figures 4(a1)–4(a3) plot three typical transmission spectra of the MBC. The time series, RF spectra, correlation curves, and PE curves of the corresponding output and input signals are plotted in columns 2–5 in Fig. 4.

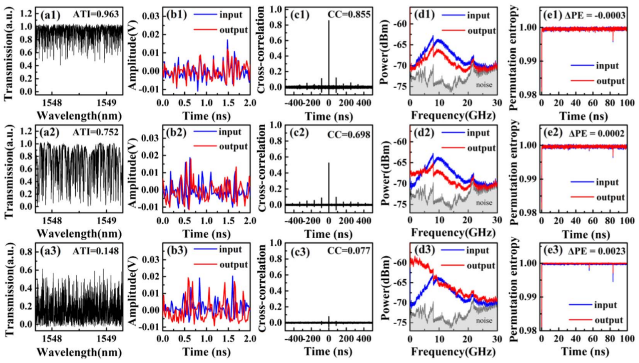

Fig. 4. (a1)–(a3) Transmission spectra of the coupling MBC with ATI = 0.963, 0.752, and 0.148. (b1)–(b3) The time series, (c1)–(c3) the cross correlation curves, (d1)–(d3) the RF spectra, and (e1)–(e3) the permutation entropy curves.

Figure 4(a1) represents a state of under coupling in which about half the light power of the resonance wavelength could couple into the cavity. The ATI is 0.963. In this case, the input-output correlation is 0.855, and the PE is slightly decreased by 0.0003. The waveform and RF spectrum of the output are similar to those of the input. The coupling point moves toward the waist of the TF, where it has the thinnest diameter, the coupling strength increases accordingly, and the bottoms of some coupling notches reach 0. Here, we call the state that the bottoms of many modes reach 0 the critical coupling state, as shown in Fig. 4(a2). The ATI is 0.752. Both the coupling strength and the mode density are larger than those of the under coupling state. The CC reduces to 0.698. The low-frequency component of the RF spectrum is flat, and the PE enhancement is 0.0003, as shown in Figs. 4(d2) and 4(e2), respectively.

The cavity moves continuously and the coupling strength will keep on increasing and achieve an over coupling state. Nearly all the pump light could couple into the cavity[28], but only some of those whose wavelength resonances with the WGMs could persist in the cavity and be coupled back to the TF, which behave as the peaks and are shown in Fig. 4(a3). In this state, most of the light on the transmission spectrum has traveled to the cavity, the ATI is low, and the filter effect on the output is evident. The RF spectrum of the output is completely different from the input one, and its CC decreases to 0.077. The energy in the RF spectrum concentrates on the low frequency in Fig. 4(d3), and the PE is clearly enhanced with the value of 0.0023.

Figure 5 shows the effects of the coupling position on the scrambling effects. The coupling position d is defined as the distance from the coupling point to the thinnest point of the TF.

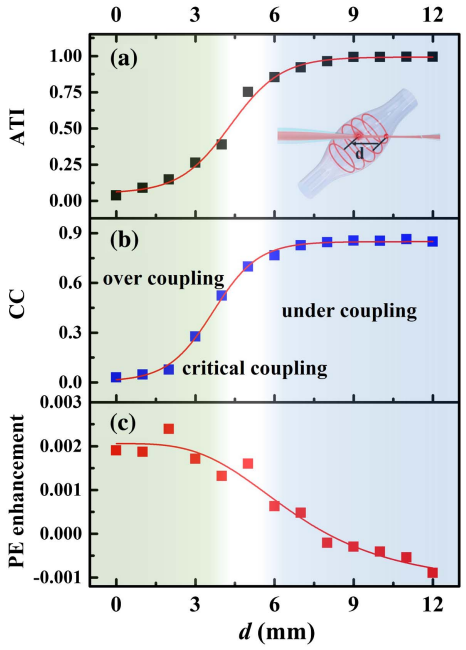

Fig. 5. (a) The ATI of the MBC, (b) the input-output correlation CC, and (c) the PE enhancement as a function of the coupling position (d), which is defined as the distance from the coupling point to the thinnest point of the tapered fiber, shown in the inset of (a).

Figure 5(a) shows that the ATI of the MBC transmission spectrum will decrease from a plateau down to another one as d reduces. As $d > 6$ mm, the ATIs are close to 0.995, denoting states of under coupling. As $d < 4$ mm, the ATIs are below 0.390, meaning over coupling states. The middle region can be treated as critical coupling states. As shown in Figs. 5(b) and 5(c), the input-output CC changes with a highly similar trend to that of the ATI, but the PE enhancement is opposite. These trends show that effective scrambling and complexity enhancement can be achieved with over coupling states. In Ref. [21], the coupling state is similar to the critical coupling in which the coupling strength is not strong enough, and the power coupled back to the TF from the cavity is low. Thus, what they achieved is time-delay signature suppression, not time-sequence scrambling.

This scrambling effect with the over coupling state could be explained by the following mechanisms. At the over coupling state, there are a lot of modes with strong coupling strength, shown as the low intensity in the transmission spectrum. Thus, the interference among the numerous modes will be strong, and the time sequence will be distorted conspicuously, which makes the cross correlation between the input and output very low and enhances the signal's complexity, i.e. the permutation entropy. However, at the under coupling state, the coupling strength is weak, and the number of modes in the transmission spectrum is small. The energy coupled back to the TF is small, and the inference among the modes is thin, which makes the scrambling effect insignificant. By increasing the coupling strength, the coupling modes will increase, and the interference, as well as scrambling effect, becomes stronger. The trends of parameters in Fig. 5 coincide with this theory. By the above analysis, the CC and the PE enhancement depend on the density of the modes, which is related to the size of the cavity, and this needs further study.

After demonstrating the waveform scrambling effects of the MBC, we should discuss some issues that remain for future work, to promote practical applications such as key distribution. According to Ref. [5], scramblers used for key distribution usually should be controllable by adjusting the parameters to produce uncorrelated outputs for identical input. The current MBC used in our experiment is a passive device and lacks tunable parameters. However, we experimentally found that the MBC output is sensitive to the polarization and the wavelength of the input. Thus, by inserting an additional polarization controller into the cavity before injection, the control of the output can be realized. The other possible way is to integrate an active device on the cavity to adjust the transmission spectrum by opto-thermal modulation[29–31]. Moreover, the over coupling state leads to a large insertion loss. Fortunately, for key distribution, the output signals are used in local to extract random bits and thus are not to be transmitted. Thus, the insertion loss can be acceptable.

3. Conclusion

In summary, we have proposed an optical scrambler based on a WGM micro-bottle cavity. Due to the interference among numerous WGMs in the cavity, efficient scrambling of the chaotic signal is realized. In the experiment, the scrambling effect under different coupling states has been analyzed and illustrated. The CC between the input and the output is only 0.028, and the PE is improved clearly. It has the advantages of low cost, simple structure, and high scrambling efficiency, and has great potential for applications such as encryption, key distribution, authentication, and optical neural calculation.

Acknowledgement

This work was supported by the National Key Research and Development Program of China (No. 2019YFB1803500), the National Natural Science Foundation of China (NSFC) (Nos. 62105233, 62035009, and 61731014), the Natural Science Foundation of Shanxi Province (Nos. 20210302124536 and 20210302123183), the Major Key Project of PCL (No. PCL2021A14), the Shanxi "1331 Project" Key Innovative Team, the Program for Guangdong Introducing Innovative and Entrepreneurial Teams, and the International Cooperation of Key R&D Program of Shanxi Province (No. 201903D421012).

References

1. A. Argyris, D. Syvridis, L. Larger, V. Annovazzi-Lodi, P. Colet, I. Fischer, J. García-Ojalvo, C. R. Mirasso, L. Pesquera, and K. A. Shore, "Chaos-based communications at high bit rates using commercial fibre-optic links," Nature **438**, 343 (2005).
2. B. Wu, Z. Wang, B. J. Shastri, M. P. Chang, N. A. Frost, and P. R. Prucnal, "Temporal phase mask encrypted optical steganography carried by amplified spontaneous emission noise," Opt. Express **22**, 954 (2014).
3. Z. Pan and L. Zhang, "Optical cryptography-based temporal ghost imaging with chaotic laser," IEEE Photon. Tech. Lett. **29**, 1289 (2017).
4. A. Uchida, R. Mcallister, R. Meucci, and R. Roy, "Generalized synchronization of chaos in identical systems with hidden degrees of freedom," Phys. Rev. Lett. **91**, 174101 (2003).
5. K. Yoshimura, J. Muramatsu, P. Davis, T. Harayama, H. Okumura, S. Morikatsu, H. Aida, and A. Uchida, "Secure key distribution using correlated randomness in lasers driven by common random light," Phys. Rev. Lett. **108**, 070602 (2012).
6. B. C. Grubel, B. T. Bosworth, M. R. Kossey, H. Sun, A. B. Cooper, M. A. Foster, and A. C. Foster, "Silicon photonic physical unclonable function," Opt. Express **25**, 12710 (2017).
7. L. Wang, D. Wang, H. Gao, Y. Guo, Y. Wang, Y. Hong, K. A. Shore, and A. Wang, "Real-time 2.5-Gb/s correlated random bit generation using synchronized chaos induced by a common laser with dispersive feedback," IEEE J. Quantum Electron. **56**, 2000208 (2020).
8. T. Yomamoto, I. Oowada, H. Yip, A. Uchida, S. Yoshimori, K. Yoshimura, J. Muramatsu, S.-I. Goto, and P. Davis, "Common-chaotic-signal induced synchronization in semiconductor lasers," Opt. Express **15**, 3974 (2007).
9. S. Sunada, K. Arai, K. Yoshimura, and M. Adachi, "Optical phase synchronization by injection of common broadband low-coherent light," Phys. Rev. Lett. **112**, 204101 (2014).
10. M. Tomiyama, K. Yamasaki, K. Arai, M. Inubushi, K. Yoshimura, and T. Uchida, "Effect of bandwidth limitation of optical noise injection on common-signal-induced synchronization in multi-mode semiconductor lasers," Opt. Express **26**, 13521 (2018).
11. H. Gao, A. Wang, L. Wang, Z. Jia, Y. Guo, Z. Gao, L. Yan, Y. Qin, and Y. Wang, "0.75 Gbit/s high-speed classical key distribution with mode-shift keying chaos synchronization of Fabry–Perot lasers," Light Sci. Appl. **10**, 172 (2021).

12. Y. Xiao, T. Deng, Z.-M. Wu, J.-G. Wu, X. D. Lin, X. Tang, L.-B. Zeng, and G. Q. Xia, "Chaos synchronization between arbitrary two response VCSELs in a broadband chaos network driven by a bandwidth-enhanced chaotic signal," Opt. Commun. **285**, 1442 (2012).
13. N. Jiang, C. Xue, D. Liu, Y. Lv, and K. Qiu, "Secure key distribution based on chaos synchronization of VCSELs subject to symmetric random-polarization optical injection," Opt. Lett. **42**, 1055 (2017).
14. A. Zhao, N. Jiang, Y. Wang, S. Liu, B. Li, and K. Qiu, "Correlated random bit generation based on common-signal-induced synchronization of wideband complex physical entropy sources," Opt. Lett. **44**, 5957 (2019).
15. C. Xue, H. Wan, P. Gu, N. Jiang, Y. Hong, and Z. Zhang, "Ultrafast secure key distribution based on random DNA coding and electro-optic chaos synchronization," IEEE J. Quantum Electron. **58**, 8000108 (2022).
16. W. Liu, Z. Yin, X. Chen, Z. Peng, H. Song, P. Liu, X. Tong, and Y. Zhang, "A secret key distribution technique based on semiconductor superlattice chaos devices," Sci. Bull. **63**, 1034 (2018).
17. R. Horstmeyer, B. Judkewitz, I. M. Vellekoop, S. Assawaworrarit, and C. Yang, "Physical key-protected one-time pad," Sci. Rep. **3**, 3543 (2013).
18. O. Buskila, A. Eyal, and M. Shtaif, "Secure communication in fiber optic systems via transmission of broad-band optical noise," Opt. Express **16**, 3383 (2008).
19. K. E. Webb, M. Erkintalo, S. Coen, and S. G. Murdoch, "Experimental observation of coherent cavity soliton frequency combs in silica microspheres," Opt. Lett. **41**, 4613 (2016).
20. D. K. Armani, T. J. Kippenberg, S. M. Spillane, and K. J. Vahala, "Ultra-high-*Q* toroid microcavity on a chip," Nature **421**, 925 (2003).
21. N. Jiang, A. Zhao, S. Liu, C. Xue, B. Wang, and K. Qiu, "Generation of broadband chaos with perfect time delay signature suppression by using self-phase-modulated feedback and a microsphere resonator," Opt. Lett. **43**, 5359 (2018).
22. M. Pöllinger, D. O'Shea, F. Warken, and A. Rauschenbeutel, "Ultrahigh-*Q* tunable whispering-gallery-mode microresonator," Phys. Rev. Lett. **103**, 053901 (2009).
23. H. Koizumi, S. Morikatsu, H. Aida, T. Nozawa, I. Kakesu, A. Uchida, K. Yoshimura, J. Muramatsu, and P. Davis, "Information-theoretic secure key distribution based on common random-signal induced synchronization in unidirectionally-coupled cascades of semiconductor lasers," Opt. Express **21**, 17869 (2013).
24. K. Zhang, Y. Wang, and Y.-H. Wu, "Enhanced Fano resonance in a non-adiabatic tapered fiber coupled with a microresonator," Opt. Lett. **42**, 2956 (2017).
25. Y. Miao, Y. Peng, Y. Xiang, M. Li, Y. Lu, and Y. Song, "Dynamic Fano resonance in thin fiber taper coupled cylindrical microcavity," IEEE Photon. J. **8**, 4502806 (2016).
26. C. Bandt and B. Pompe, "Permutation entropy: a natural complexity measure for time series," Phys. Rev. Lett. **88**, 174102 (2002).
27. L. Zunino, O. A. Rosso, and M. C. Soriano, "Characterizing the hyperchaotic dynamics of a semiconductor laser subject to optical feedback via permutation entropy," IEEE J. Sel. Top. Quantum Electron. **17**, 1250 (2011).
28. M. Cai, O. Painter, and K. J. Vahala, "Observation of critical coupling in a fiber taper to a silica-microsphere whispering-gallery mode system," Phys. Rev. Lett. **85**, 74 (2000).
29. S. Zhu, L. Shi, S. Yuan, X. Xu, and X. Zhang, "All-optical control of ultrahigh-*Q* silica microcavities with iron oxide nanoparticles," Opt. Lett. **42**, 5133 (2017).
30. S. Zhu, L. Shi, B. Xiao, X. Zhang, and X. Fan, "All-optical tunable microlaser based on an ultrahigh-*Q* erbium-doped hybrid microbottle cavity," ACS Photonics **5**, 3794 (2018).
31. S. Zhu, W. Wang, L. Ren, C. Gong, Y.-C. Chen, L. Shi, and X. Zhang, "Thermal gradient induced transparency and absorption in a microcavity," Laser Photon. Rev. **17**, 2200644 (2023).